Facies prediction with Bayesian inference: Application of supervised and semisupervised deep learning

Sagar Singh*, Ilya Tsvankin*, & Ehsan Zabihi Naeini†
*Center for Wave Phenomena and Dept. of Geophysics, Colorado School of Mines, Golden CO 80401
†Earth Science Analytics, London
email: sagarsingh@mines.edu

ABSTRACT
Delineation of geologic facies from seismic reflection data plays an important role in reservoir characterization during hydrocarbon exploration and development. Facies classification is often done manually by an experienced interpreter, which makes this process subjective and inefficient. Several machine-learning (ML) models have been proposed to automate multiclass facies segmentation but significant practical challenges still remain (e.g., limited scope of training data with labels, imbalanced class distribution, lack of rigorous performance evaluation metrics, etc). We present supervised and semisupervised Bayesian deep-learning methodologies designed to improve analysis of seismic facies depending on the scope of the labeled data. The developed networks reliably predict facies distribution using seismic reflection data and estimate the corresponding uncertainty. Therefore, they provide more consistent and meaningful information for seismic interpretation than commonly used deterministic approaches. Two deep neural networks are successfully tested on seismic data from the Dutch sector of the North Sea. In the case of sufficient availability of manually interpreted labels (or facies), the supervised learning model accurately recovers the facies distribution. When the amount of the interpreted labels is limited, the semisupervised algorithm is efficiently applied to avoid overfitting.

Key words: Modified UNet, Attention gate, Bayesian inference, F3 data

1 INTRODUCTION

A reservoir in the geosciences represents a natural storage unit of fluid or gas in the subsurface. Reservoirs that contain oil or gas are of primary interest in hydrocarbon exploration. Characterizing the often complex reservoir structure is a challenging task that requires time-consuming manual interpretation performed by experienced geologists and geophysicists. With a continued increase in the volume of seismic data, the reliance on human interpretation renders this procedure subjective and inefficient (Bond et al., 2007).

Accurate automatic interpretation of lithologic units from seismic reflection data could significantly enhance subsurface characterization workflows. Over the past decade, several machine-learning (ML) models have been proposed for efficient lithologic interpretation. Examples of such ML algorithms include:

- $K-$means clustering (Napoli et al., 2020).
- Support vector machines (Zhao et al., 2014; Wrona et al., 2018, Singh et al., 2021).
- Self-organizing maps (Strecker and Uden, 2002; de Matos et al., 2006; Saraswat and Sen, 2012; Zhao et al., 2017).
- Generative topographic mapping (Roy et al., 2014).
- Independent component analysis (Lubo-Robles and Marfurt, 2019).
- Artificial neural networks (ANNs) based on different seismic attributes (West et al., 2002; Saggaf et al., 2003; Singh et al., 2016).

The above methodologies operate with different seismic attributes, whose quality is often difficult to evaluate.

The recent progress in computational resources (including graphical processing units or GPUs), has made it feasible to use deep-learning models for seismic interpretation (Guitton, 2018; Shi et al., 2019). In particular, deep-learning networks have the potential to provide highly efficient semantic segmentation because they are capable of extracting essential features in high-dimensional spaces from large-scale data sets.

Although most convolutional networks learn pointwise estimates of their weights, such estimates do not fully encapsulate the uncertainty inherent in the weight values. Describing the weights of the neural networks as probability distributions has several implications. First, the network becomes nondeterministic; every time one computes a forward pass, each weight distribution has to be sampled to obtain a point estimate, which can be used for computing the inference. Repeated applications of this sampling technique, called Monte Carlo sampling, results in different predictions, which can then be analyzed to evaluate the uncertainty. Second, such network is much more difficult to train (especially in 3D), and it is more susceptible to vanishing/exploding gradients of the employed loss function. Here, we use an innovative normalization technique called group normalization (Wu and He, 2018) to solve this problem, as discussed below.

Our Bayesian architecture draws from the image segmentation literature by utilizing the common encoder-decoder setup from UNet (Ronneberger et al., 2015). In this architecture, the encoder half of the network compresses the input into a latent space, whereas the decoder half decompresses the latent representation of the input into a segmentation map.

Although deep learning has become increasingly popular in geophysics, implementation of 2D/3D facies classification is hampered by such issues as insufficient labeled data available for training, imbalanced facies class distribution, and lack of rigorous criteria for performance evaluation. Besides, the facies class distribution in the training set is not always consistent with field data. We show how to address these challenges using a facies model derived from North Sea field data.

Because the amount of well data can vary from relatively abundant in older fields to scarce in new prospects, we propose two types of deep-learning workflows. The first is a state-of-the-art Attention-gated modified UNet convolutional model, which relies on a sufficient scope of labeled data. The second is a semisupervised general adversarial network (GAN) which requires only limited labeled data to be incorporated in the training process (Salimans et al., 2016). Both approaches use probabilistic convolutional layers that can measure errors in the weight space. This results in statistically justified uncertainty quantification at the cost of at least doubling the number of trainable parameters and increasing the convergence time, as well as the sensitivity to hyperparameter optimization. Due to the proper handling of randomness in the convolutional layers, the predicted facies models are more consistent with the geologic structure and reflection data compared to the conventional methods.

The paper starts by discussing supervised and semisupervised deep-learning methodologies and the proposed architecture modifications. Then we describe the loss functions designed to generate an accurate posterior distribution of network weights and the geologic model employed to test the proposed networks. The methodology is applied to publicly available field data from the North Sea. The consistency of the results from both networks confirm the generalization capabilities of our models.

2 METHODOLOGY

The proposed supervised and semisupervised ML models include two main components: Attention layers and uncertainty estimation using Bayesian inference. We present "end-to-end" models designed to operate with raw seismic data and generate comprehensive facies classification results along with the associated uncertainties. Below we describe the architecture of both models and the key steps in implementing supervised and semisupervised learning.

2.1 Supervised training model

Supervised learning is designed to learn a function that maps input examples to an output label based on training data-label pairs. It employs labeled training data to establish a nonlinear relationship between the desired output and the input that includes a set of training examples (Mohri et al., 2012).

Deep-learning convolutional neural networks (CNN) are commonly applied to computer vision (Krizhevsky et al., 2012) and natural language processing. They are fashioned after the neuron connectivity patterns in human brain, and represent a regularized version of multilayer perceptrons in fully connected networks.

Generally, a CNN is made up of one input layer, multiple hidden layers, and an output layer. The types of hidden layers include convolutional, ReLU (activation function), pooling, fully connected dense, and normalization layers. Deep-learning CNNs outperform the existing methods discussed above due to their effectiveness and minimal preprocessing requirements compared to other image-processing techniques. The mechanism of hierarchical feature learning enables CNNs to capture the most salient and sensitive feature representations for a range of problems, such as image classification and segmentation. A CNN is different

from regular neural networks (e.g., the multilayer perceptron or MLP) because it uses multiple convolutional layers instead of fully connected layers to filter input data.

CNNs take advantage of the fact that a pixel is more closely related to its neighbors than to more distant locations by connecting each neuron to just a local region of the input volume. Thus, CNNs models are more computationally efficient than fully connected MLPs. Because seismic volumes can be regarded as a particular type of image, we investigate the feasibility and performance of CNNs in seismic facies segmentation. Typically, facies information is derived from well logs and core analysis. If there is a sufficient number of samples with labels, seismic facies interpretation can be formulated as a supervised classification problem.

Models commonly used in image segmentation problems represent variations of UNet (Ronneberger, 2015) and include the extra localization step to increase the training time and the number of model parameters. The accuracy of model segmentation strongly depends on the implementation of the first positioning step. To address the need for more accurate segmentation of images, we employ the attention-gated modified UNet, a reliable segmentation model that combines the UNet architecture with an attention mechanism (Li et al., 2020). The elements of the employed architecture are described below.

2.1.1 Modified UNet architecture

UNet has been widely applied to image segmentation problems with some modifications for different segmentation tasks. Figure 1a shows a schematic representation of our modified UNet architecture, which employs an encoder-decoder setup. The encoder (left) half of the network compresses the input into a latent space while the decoder (right) half decompresses the latent representation of the input into a segmentation map. The encoder half includes four stages, each with two convolutional and normalization layers followed by a max-pooling layer to reduce the size of the input. Thus, after each layer, the input's depth and height are halved, which reduces the input size by a factor of four.

The decoder half of the network consists of three stages corresponding to the first three layers of the encoder half. First, we upsample the output of the previous layer and use convolutional and normalization layers to double the depth and height of the input. The output from the earlier step is then concatenated with the prepooling output of the corresponding encoder layer; such skip connection facilitates feature-forwarding through the network (Figure 1a). This is followed by application of two more convolutional and normalization layers, the final convolutional layer, and a softmax activation. The resulting volume represents a multiclass segmentation probability map and has the same size as the input.

2.1.2 Attention Gate Signal

To bridge the results of seismic facies with the input label attributes (features), we employ the attention mechanism strategy (Figure 1b). Attention-gated networks are designed to learn feature-attention probabilities (Oktay et al., 2018). Likewise, we compute attention maps to highlight the regions in the seismic image that contribute to the facies-segmentation process. In addition to the benefits of interpretability, the attention mechanism enforces suppression of the interference from untargeted information (Li et al., 2021).

2.1.3 Bayesian inference

A probabilistic approach to deep learning makes it possible to account for uncertainty, so that lower levels of confidence can be assigned to inaccurate predictions. The sources of uncertainty in the data include measurement errors or noise in the labels ("aleatoric" uncertainty) or in the model, as well as insufficient data availability for effective learning ("epistemic" uncertainty).

Bayesian deep learning allows one to compute epistemic uncertainties by modeling a posterior distribution $P(\mathbf{w}|\mathcal{D})$ over the network weights $\mathbf{w}$ for a given training set of data images and labels ($\mathcal{D}$). In practice, finding the exact posterior is not feasible, but an approximation $q(\mathbf{w}|\theta)$ can be obtained using the so-called variational inference (θ is a variational parameter) by minimizing the Kullback-Leibler (KL) divergence (Graves, 2011). This approach optimizes the weights to prevent overfitting, while simultaneously modeling the weights distribution. The resulting outputs can then be averaged to recover the segmentation, and the standard deviation between samples can serve as an estimate of the epistemic uncertainty.

The uncertainty evaluation enhances the interpretability of the model (Figure 1a). Each convolutional Bayesian layer is initialized with a standard normal prior $P(\mathbf{w}) = \mathcal{N}(0, 1)$ and employs a flipout estimator (Wen et al., 2018) to approximate the posterior distribution during forward passes. The flipout estimator provides a Monte Carlo approximation of the posterior distribution by integrating over the Bayesian layer's kernel and bias, which significantly lowers the variance (Wen et al., 2018). Bayesian layers are not included in the encoder half of the network to enhance the information transfer between the original input and the latent space (LaBonte et al., 2020).

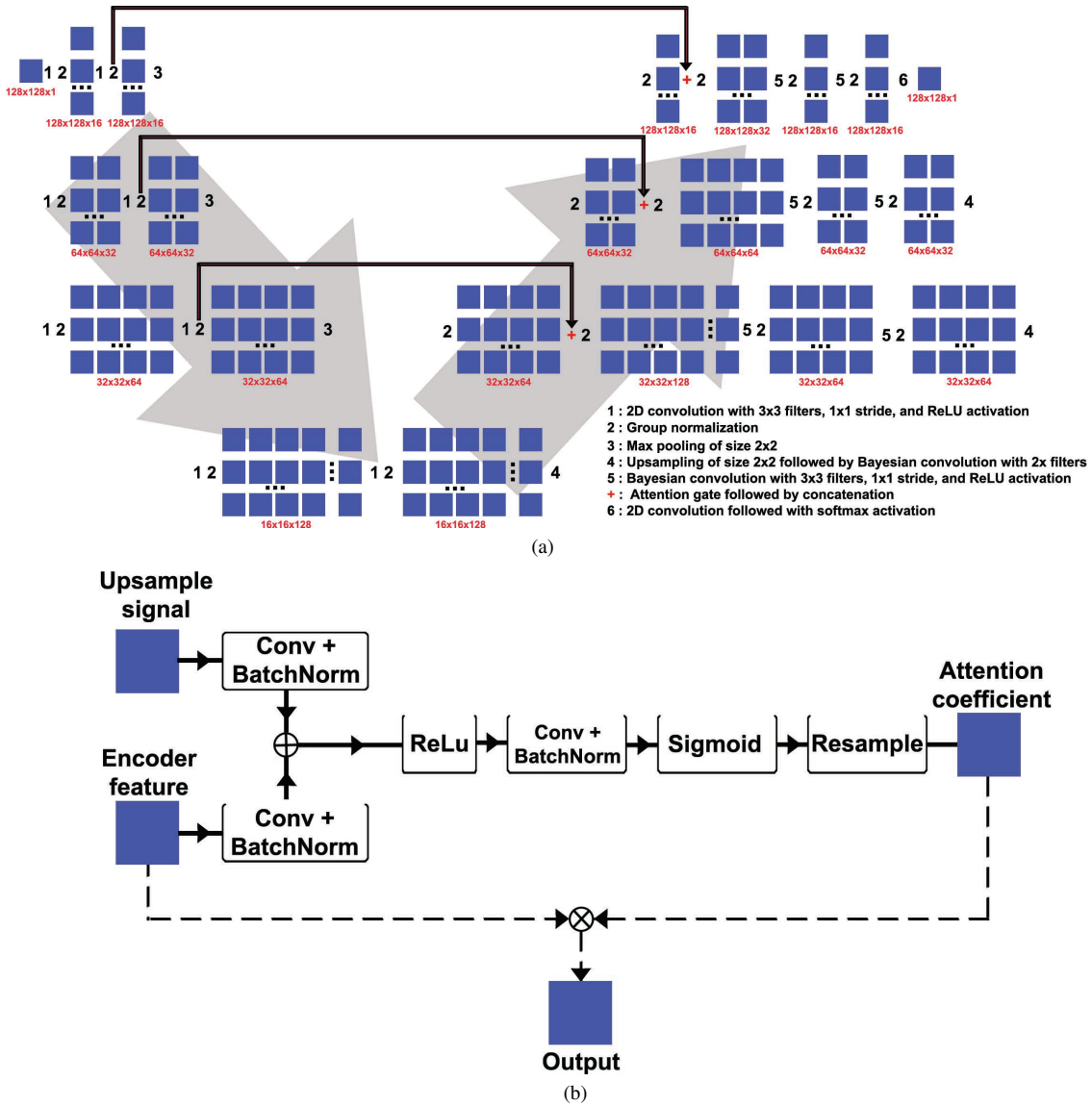

Figure 1. (a) Schematic of the modified UNet architecture. The measurements are depth, height, and channels. (b) Attention gate signal.

2.1.4 Loss function and optimizer

We use monotonic KL annealing (Bowman et al., 2016) to improve the convergence of the model because it helps learn the segmentation before applying the KL divergence penalty. We denote the current epoch as E and define the following hyperparameters: the KL starting epoch s, the KL initial weight k_0, and the step value k_1. Then the KL weight for the current epoch k_E is given by:

$$k_E = \begin{cases} k_0 & \text{if E} \leq \text{s}, \\ \min[1, k_0, +k_1(E-s)] & \text{if E} > \text{s}. \end{cases} \tag{1}$$

Variational learning finds the parameters θ of the distribution $q(\mathbf{w}|\theta)$ by minimizing the variational free-energy cost function $\mathcal{F}$, often called the "expected lower bound" (ELBO). That function (Blundell et al., 2015) consists of the sum of the KL divergence and the negative log-likelihood (NLL):

$$\mathcal{F}_i^E(\mathcal{D}_i, \theta) = \frac{k_E}{M} KL[q(\mathbf{w}|\theta)||P(\mathbf{w})] - E_{q(\mathbf{w}|\theta)}[\log P(\mathcal{D}_i|\mathbf{w})], \tag{2}$$

where M is the total number of training examples, and i is the minibatch. We divide the KL (Kullback–Leibler) divergence term by M to optimize the mini-batch $i \in \{1,2,...M\}$, as proposed by Graves (2011). This distributes the KL divergence penalty evenly over each mini-batch; without this scaling, the KL term dominates equations 1 and 2, causing the model to converge to a posterior with suboptimal accuracy. Equation 2 can be interpreted as a tradeoff between satisfying the simplicity prior (the KL term) and fitting the data set (NLL term).

2.2 Semisupervised training model

Semisupervised learning combines a small volume of labeled data with a larger amount of unlabeled data during training procedure. This training model falls between unsupervised learning (with no labeled training data) and supervised learning (with only labeled training data). Unlabeled data can significantly improve learning accuracy when combined with even a small number of labeled data points. The acquisition of labeled data for a learning problem often requires a skilled human agent or a physical experiment. Hence, the cost of the labeling process may prohibit employing large, fully labeled training sets, whereas the acquisition of unlabeled data is relatively inexpensive. In such situations, semisupervised learning can provide great practical value. Semisupervised learning is also of theoretical interest in ML, especially as a model for human learning.

The Generative Adversarial Network (GAN) is an architecture that makes effective use of large, unlabeled data sets to train an image generator model (G) via a discriminator (D). In some cases, the discriminator model can be used as a starting point for developing a classifier. The semisupervised GAN (or SGAN) model is an extension of the GAN architecture that involves simultaneous training of a supervised discriminator, an unsupervised discriminator, and a generator model. Unlike traditional neural networks, GANs comprise two competing components, each represented by a neural network: the generator and discriminator. The generator creates samples that come from a targeted, yet unknown, probability distribution (for instance, data points from a Gaussian distribution or channelized reservoir realizations) using random noise in a low-dimensional space as the input. In contrast, the discriminator is trained to predict whether a given image is real (i.e., obtained from the data) or fake (generated), allowing it to learn features from unlabeled images. Eventually, the generator evaluates the data's underlying probability distribution and starts producing samples with realistic appearance. The result is a supervised classification model that provides accurate generalization to yet unused examples and a generator model that outputs plausible image examples from the input data. A general architecture of a semisupervised GAN is illustrated in Figure 2.

The discriminator model in the semisupervised GAN is updated to predict K+1 classes, where K is the number of classes in the prediction problem and the additional label is added for a new "fake" class. It involves direct training of the discriminator model for both the unsupervised GAN task and the supervised classification task simultaneously. As such, the discriminator is trained in two modes (supervised and unsupervised).

Unsupervised Training: In the unsupervised mode, the discriminator is trained in the same way as the traditional GAN to predict whether the example is either real or fake.

Supervised Training: In the supervised mode, the discriminator is trained to predict the class label of real examples. Training in the unsupervised mode allows the model to learn useful feature extraction capabilities from a large unlabeled data set, whereas during supervised training the model uses the extracted features and applies class labels.

Consider a standard model for classifying a data point x into one of K possible classes. The output of the classifier is a K-dimensional vector that can be turned into the class probabilities by applying softmax. The classic GAN (Salimans et al., 2016) is implemented by labeling samples from the GAN generator G with a new "generated" class K + 1. We use $P_D(y \leq K|x)$ and $P_D(K+1|x)$ to determine the probability that x is true or false, respectively. The model D is both a discriminator and a classifier, which increases the dimension of the output from K to K +1. Thus, the discriminator D is defined as

$$P_D(k|x) = \frac{exp\left[\boldsymbol{\omega}_k^T \mathbf{f}(x)\right]}{\Sigma_{i=1}^{K+1} exp\left[\boldsymbol{\omega}_i^T \mathbf{f}(x)\right]}, \tag{3}$$

where $\mathbf{f}(x)$ is a nonlinear vector-valued function, $\boldsymbol{\omega}_k$ is the weight vector for class k and $\{\boldsymbol{\omega}_1^T \mathbf{f}(x), ..., \boldsymbol{\omega}_{K+1}^T \mathbf{f}(x)\}$ is the (K + 1)-dimensional vector. Since a discriminator with K + 1 outputs is overparameterized, ω_{K+1} is fixed as a zero vector. We also denote $D := (\omega, f)$ as a discriminator. Similar to the traditional GANs, D and G solve the following two-component minimax problem with the value function J_{GD}:

$$\min_G \max_D J_{GD} = \min_G \max_D (L_D + U_{GD}), \tag{4}$$

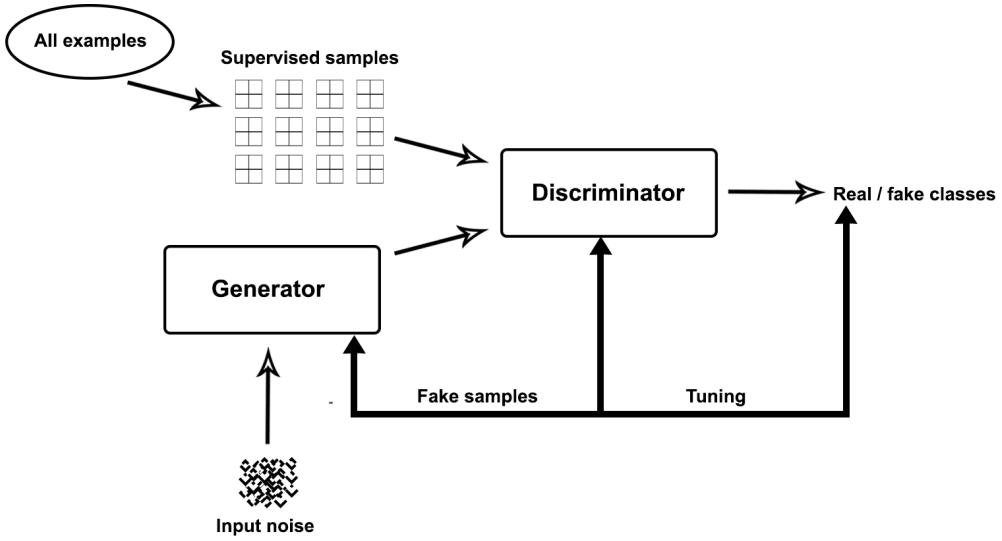

Figure 2. Architecture of the semisupervised GAN includes the generator and the discriminator; both use the network architecture from Figure 1.

where

$$L_D =_{(x,y)\sim p(x,y)} \log P_D(y|x, y \leq K), \tag{5}$$

$$U_{GD} =_{x\sim p(x)} \log P_D(y \leq K|x) +_{x\sim p_G(x)} \log P_D(K + 1|x). \tag{6}$$

Here L_D is the supervised learning objective for all labeled data and U_{GD} is the unsupervised (i.e., the traditional GAN) objective, in which p is the true data distribution and p_G is the generated distribution. When G is fixed, the objectives J_{GD} and U_{GD} become J_D and U_D, respectively. After obtaining a satisfactory value of D by optimizing J_{GD}, we use $\operatorname{argmax} P_D(k|x, k \leq K)$ to determine the class of the input data x. Similar to other existing semisupervised GAN algorithms, L_D is used as the supervised learning objective by applying only the softmax operator to the former K-dimensional vector of the output of D.

The result is a classifier model that can achieve high-fidelity results for standard problems after training on a small number of labeled examples (up to a thousand). Additionally, the training process can produce realistic, high-quality images from the generator model.

2.2.1 Stacked Discriminator Models With Shared Weights

The proposed GAN architecture involves creating separate unsupervised and supervised models but it attempts to reuse the output layers of one model as the input into the other model. Salimans et al. (2016) describe an efficient implementation of this approach, where the supervised model is created with K output classes and a softmax activation function. Then the unsupervised model uses the output of the supervised model prior to the softmax activation to calculate a normalized sum of the exponential outputs.

3 FIELD-DATA APPLICATION

The North Sea is rich in hydrocarbon deposits and well studied in the geophysical and geologic literature (Doornenbal, 2014). The continental shelf of the North Sea offshore the Netherlands is divided into zones denoted by different letters of the alphabet; smaller areas within those zones are marked with numbers. Here, we use data from one of such areas, a 16 km x 24 km rectangle known as the F3 block. A 3D seismic survey was conducted in 1987 to identify the geologic structures in the F3 block and search for hydrocarbon reservoirs. In addition, a large number of boreholes was drilled inside the F3 block over the years. The data from the 3D seismic survey, along with additional products, were made publicly available by dGB Earth Sciences in 2020.

Using inline 339 from the survey, ConocoPhillips identified nine groups of facies (the labeled data are freely available). Eight facies have distinct patterns in seismic reflection images and one more facies is used to represent the rest of the labeled samples. These facies along with their main lithostratigraphic features are shown in Figure 3 and listed in Table 1.

To demonstrate the performance of the proposed deep neural networks in seismic facies classification, we apply them to the

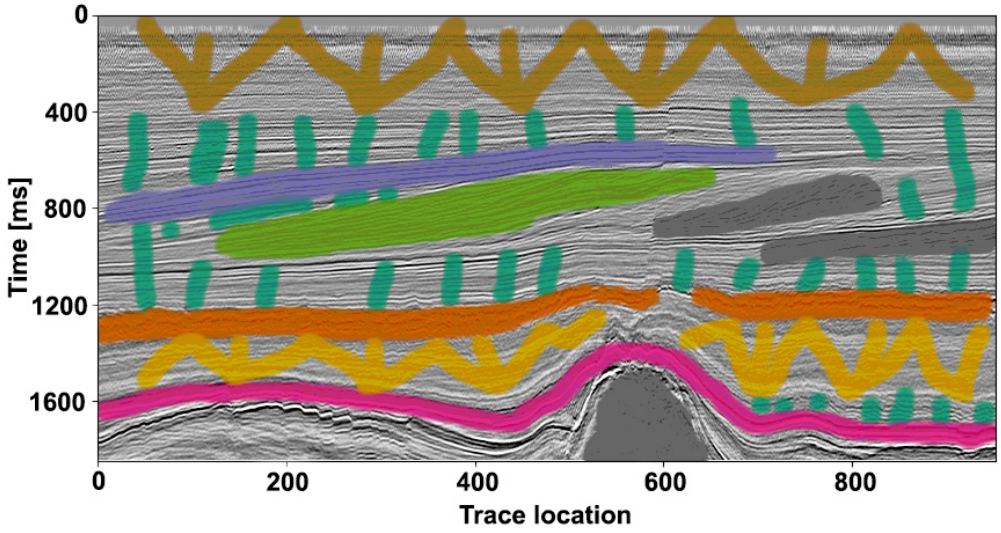

Figure 3. Labeled data set from a 2D inline time-migrated seismic section. Color interpretations are defined in Table 1.

Facies	Seismic reflection characteristic
1. Brown	Low coherency
2. Violet	High-amplitude continuous
3. Grass green	Low-amplitude dips
4. Gray	High-amplitude dips
5. Orange	Chaotic
6. Yellow	Low amplitude
7. Magenta	High amplitude
8. Gray	Salt intrusion
9. Turquoise	Everything else

Table 1. Facies identified by ConocoPhillips from the seismic data for the F3 block. The facies names are taken from Liu et al. (2020).

field data from the F3 block. We parallelize both developed networks and train them on four NVIDIA Tesla V100 GPUs, each with 12GB of memory.

3.1 Supervised facies prediction

We generate 128,000 training examples by separating the interpreted slice into patches of size 128x128 with the corresponding labels; 30,000 random samples are set aside for validation (Figure 4). Such a large number of diverse labeled samples makes it possible to perform classification using the developed supervised network. To avoid overfitting and extend the network's generalization capabilities, we employ data augmentation that increases the diversity of the training set through application of such random transformations as image rotation, rescaling, shifting, and zooming.

Besides the attention mechanism, Bayesian layers are introduced in the decoder to sample the posterior distribution and obtain meaningful uncertainty maps, which can be directly interpreted as the confidence intervals for the segmentation. Because seismic facies are generally more continuous horizontally than vertically, the pooling size in the supervised model is doubled along the horizontal axis.

Figure 5 shows the training history using the Adam optimizer (Kingma and Ba, 2015) with a batch size of 64 and a dynamic learning rate that has the 0.001 starting value. Based on the training history, we stop training at approximately 20 epochs to minimize the possibility of overfitting. The prediction pixel and IOU (Appendix A) accuracy for the validation set is above 99.9%.

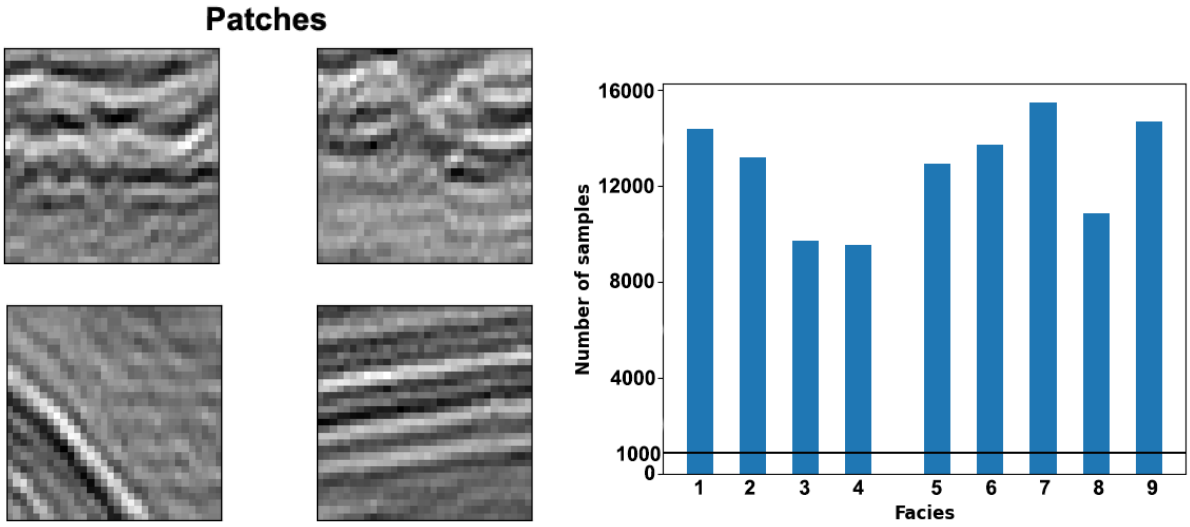

(a) (b)

Figure 4. Training data for the ML model. (a) Examples of patches extracted from the input data, and (b) the distribution of labels for each available facies. One thousand samples for each class (marked by the horizontal line on plot b) are used in the semisupervised learning model.

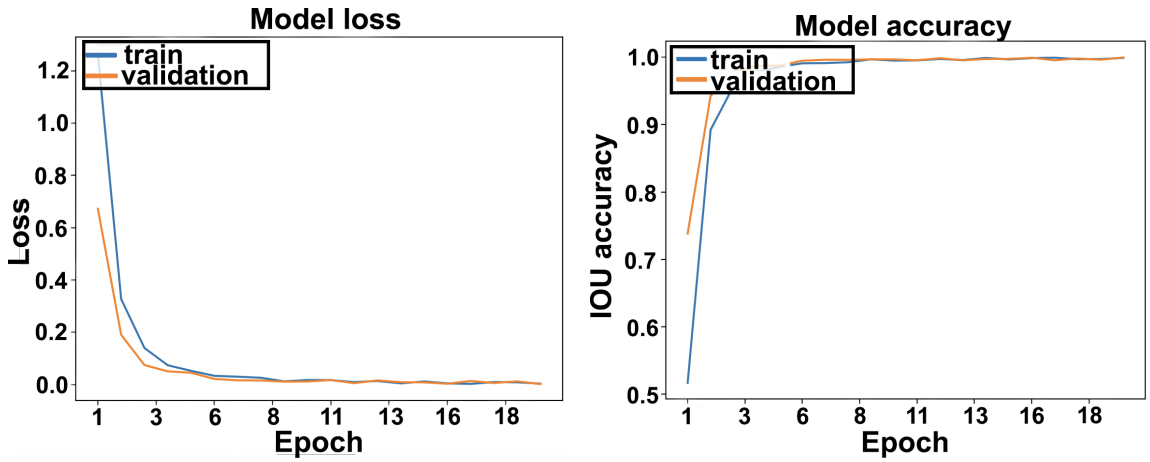

Figure 5. Model training history for the supervised learning.

The employed accuracy metrics are particularly useful to evaluate the model performance for strongly imbalanced data sets. After successfully training and evaluating the networks, we perform facies prediction for xline 779 (Figure 6). The classification results overlaid on the seismic image (Figure 7) indicate that the predicted target facies distribution is consistent with the seismic data.

To obtain a distribution of the posterior for each grid point, 50 Monte Carlo samples are computed in the rectangular region marked in Figure 7. We define the confidence intervals for the segmentation as the 33rd and the 67th percentiles of the softmax values and the uncertainty as the difference between these percentiles (Figure 8). Note that the uncertainty maps from our Bayesian model provide consistent error estimates across the boundaries of the facies.

3.2 Semisupervised facies prediction

Supervised training models perform adequately, if a sufficient volume of borehole data is available. However, supervised learning may fail in areas with just a few drilled wells, where the model becomes overfitted due to a small number of the training data samples. This limits the applicability of supervised algorithms, especially in new exploration areas.

The same model architecture as in the supervised example is used here to demonstrate the feasibility of applying semisuper-

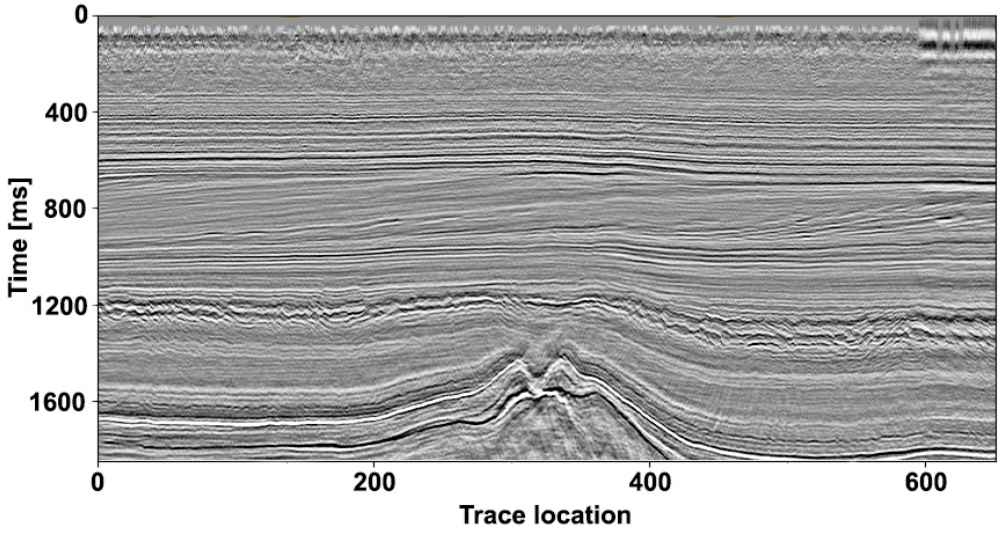

Figure 6. Xline 775 from the F3 block.

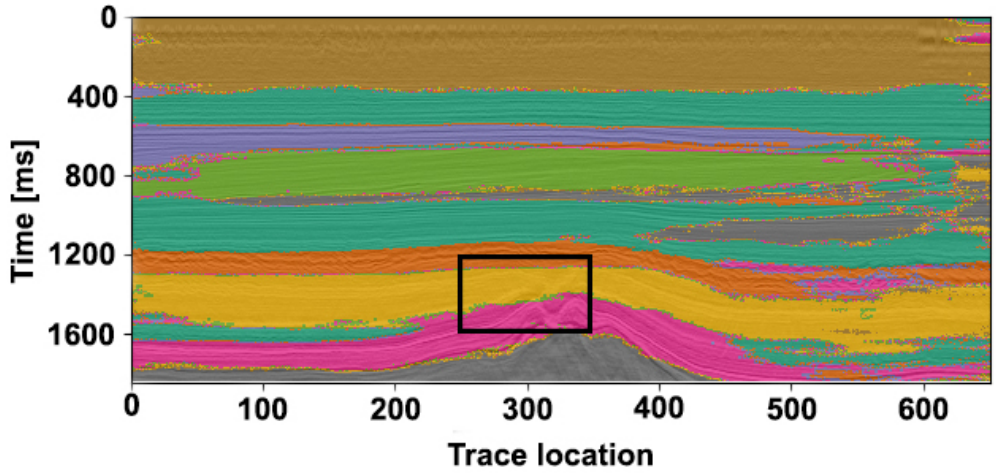

Figure 7. Facies prediction for xline 779 using the supervised training model. The uncertainties are estimated inside the marked rectangular area.

vised GAN to facies classification with a relatively small number of the available labeled data points. We extract 64x64 patches from the interpreted slice and select 1,000 training samples for each corresponding label, as opposed to a total of 128,000 samples in the supervised training above. The reason for the smaller patch size in semisupervised learning is the increase in the memory requirements caused by incorporating the complex network architecture (Figure 1) for both the generator and discriminator. The generator takes patches of Gaussian realizations as the input to synthesize data with the same size as the training samples (64×64×1).

We train the generator and discriminator networks on labeled samples extracted randomly from all possible examples and on unlabeled samples evenly extracted from the seismic data along the same inline. In the inference phase, the generator is discarded, and the discriminator is used for the final prediction. The training is stopped at approximately 20 epochs to avoid overfitting (Figure 9).

The classifier's prediction accuracy on the full data set exceeds 99%. The facies are predicted again for xline 779, and the classification results are overlaid on the seismic data (Figure 10). Compared to the supervised learning results, the semisupervised prediction model is more coherent in the deeper part of the section (for times > 1.1 s). The results further improve as the number of the labeled training examples and the patch size are increased (which requires more computing time and memory).

As before, 50 Monte Carlo samples in the marked rectangular region are employed to generate uncertainty maps. The confidence intervals for the segmentation results are set between the 33rd and 67th percentiles of the softmax values (Figure 11).

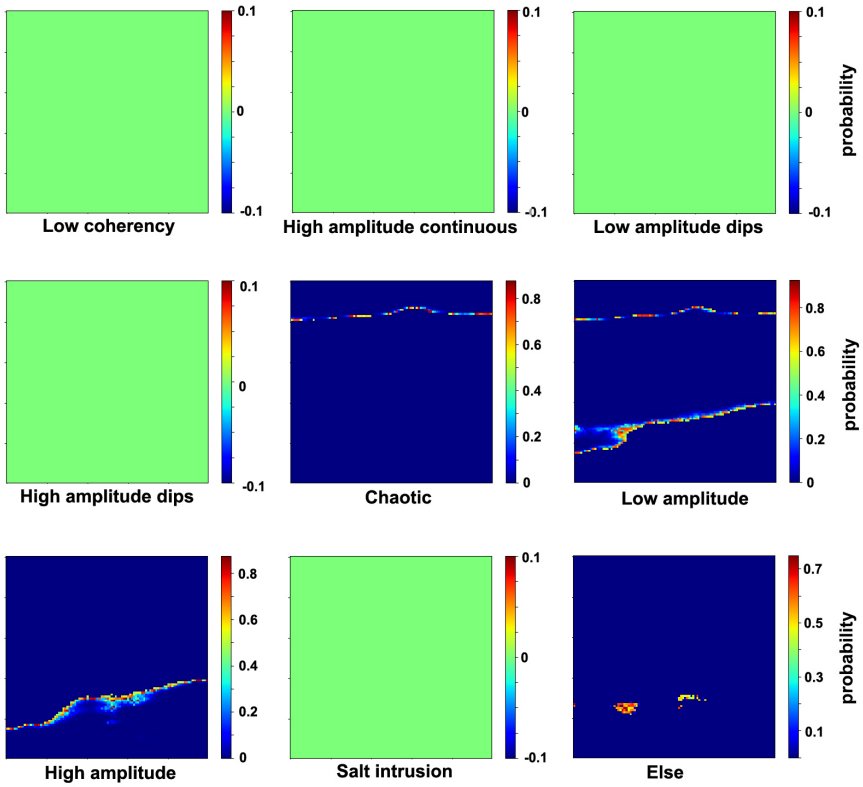

Figure 8. Supervised uncertainty maps of the posterior prediction for the confidence interval between 30-70%. Uncertainties are observed mostly along the boundaries between facies.

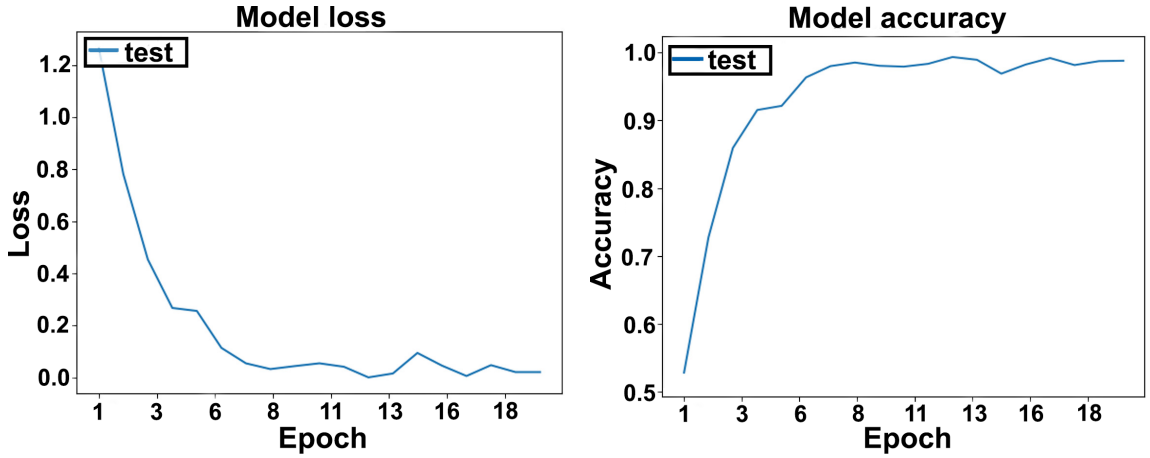

Figure 9. Model training history for the semisupervised learning.

4 DISCUSSION

The stochastic nature of machine-learning algorithms is an important foundational concept in machine learning, which needs to be understood for effective interpretation of the behavior of predictive models. 3D imaging techniques provide the ability to map the interior of objects (e.g., geologic formations) which cannot be studied otherwise. In particular, 3D facies models help interpret the depositional environment and spatial facies distribution using reflection seismic data, which is extremely important in hydrocarbon exploration and development. A critical step in the facies analysis is segmentation, often performed by manually labeling each

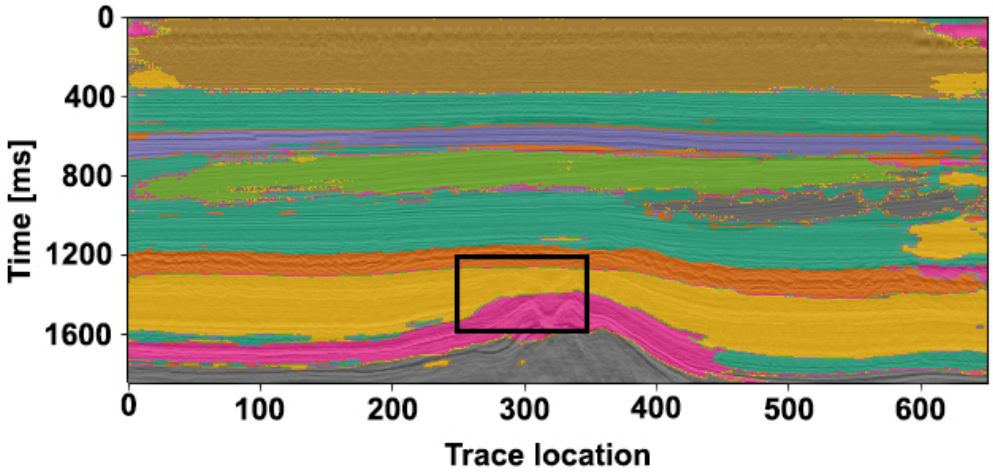

Figure 10. Facies prediction for xline 779 using the semisupervised training model.

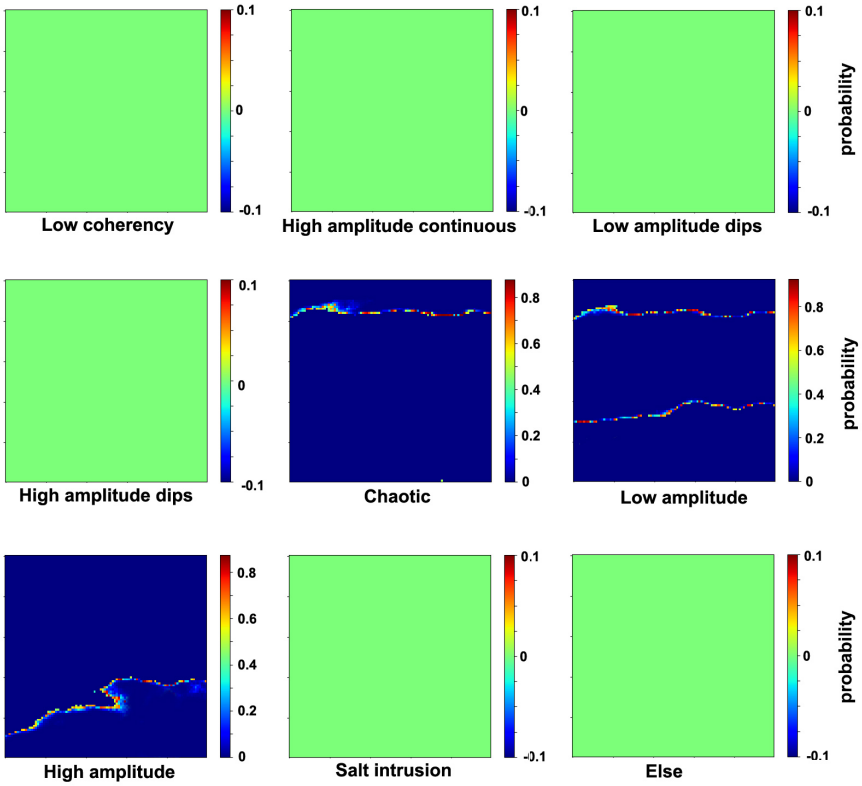

Figure 11. Semisupervised uncertainty maps. According to the supervised uncertainty estimates, the "else" facies has zero probability in that region.

voxel in a seismic reflection image. However, due to various artifacts and noise in field data, manual segmentation is expensive, irreproducible, and subject to human error.

Deep-learning models, such as convolutional neural networks (CNNs), have revolutionized automated segmentation of 3D images by providing a fast and accurate solution to these problems. For effective application to hydrocarbon exploration, segmentation must include uncertainty quantification that yields accurate confidence intervals for drilling projects.

The Bayesian inference models proposed here evaluate the uncertainty in the weight space. This results in statistically-justified uncertainty quantification at the cost of at least doubling the number of trainable parameters (Gal and Ghahramani, 2016) and in-

creasing the convergence time and sensitivity to hyperparameter optimization (Ovadia et al., 2019). Our Bayesian models effectively predict multiclass segmentation and generate credible uncertainty maps, which can be directly interpreted as the confidence intervals for the segmentation. Although we have leveraged many ideas from previous ML research, the paper presents a new implementation of deep learning for facies classification.

5 CONCLUSIONS

Classification of seismic facies is an important interpretation step because it helps visualize and evaluate different geologic settings using reflection data. We present two types of deep neural-network workflows designed for efficient automatic facies analysis. Fully supervised convolutional networks are preferable for mature fields with an abundance of labeled data, whereas semisupervised GANs perform better for new prospects with a limited number of labels. Also, we added an attention scheme to our architecture to generate superior segmentation results. Both proposed models support Bayesian inference, which generates statistically justified uncertainty maps. By estimating the uncertainty in the weight space, the employed Bayesian scheme provides interpretable error quantification for segmentation problems. Both models were successfully tested on seismic field data from the North Sea, which confirms the significant potential of deep-learning methods in quantitative seismic interpretation. Our results demonstrate that deep learning provides a robust framework for combining well information and 3D seismic data in automated interpretation of seismic facies.

6 ACKNOWLEDGMENTS

This work was supported by the Consortium Project on Seismic Inverse Methods for Complex Structures at the Center for Wave Phenomena (CWP). The data used in this study can be accessed at “https://github.com/bolgebrygg/-MalenoV”.

7 APPENDIX A

8 EVALUATION METRICS

To objectively evaluate the performance of our models on field data, we use the evaluation metrics that are described in the computer-vision literature. If the set of pixels belonging to class i is denoted by G_i, and the set of pixels in class i by F_i, the correctly classified pixels form the set $G_i \cap \mathrm{F}_i$.

The first evaluation metric is the Pixel Accuracy (PA) that represents the percentage of the correctly classified pixels over all classes:

$$PA = \frac{\sum_i |F_i \cap G_i|}{\sum_i |G_i|}, \tag{A-1}$$

where $|\cdot|$ denotes the number of elements in a set.

The second metric is the Intersection over Union (IOU), which is the number of elements of the intersection of G_i and F_i normalized by the number in elements of their union set,

$$IOU_i = \frac{|F_i \cap G_i|}{|F_i \cup G_i|}. \tag{A-2}$$

This metric quantifies the overlap between the two sets and should be equal to unity if and only if all pixels were correctly classified. Averaging the IOU over all classes yields the Mean Intersection over Union (Mean IOU),

$$\text{mean } IOU_i = \frac{1}{n_c} \sum_i IOU_i. \tag{A-3}$$

REFERENCES

Bowman, S.R., L. Vilnis, O. Vinyals, A. M. Dai, R. Jozefowicz, S. Bengio, 2016, Generating sentences from a continuous space: Conference on Computational Natural Language Learning, 10-21, doi: 10.18653/v1/K16-1002.

Bond, C. E., A. D. Gibbs, Z. K. Shipton, and S. Jones, 2007, What do you think this is? "Conceptual uncertainty" in geoscience interpretation: GSAToday, **17**, no. 11, 4–10, doi: 10.1130/GSAT01711A.1.

Blundell, C., J., Cornebise, K., Kavukcuoglu, D., Wierstra, 2015, Weight uncertainty in neural networks: International Conference on Machine Learning, **37**, 1613-1622.

de Matos, M. C., P. L. Osorio, and P. R. Johann, 2006, Unsupervised seismic facies analysis using wavelet transform and self-organizing maps: Geophysics, **72**, no. 1, P9–P21, doi: 10.1190/1.2392789.

Gal, Y., Z., Ghahramani, 2016, Dropout as a bayesian approximation: Representing model uncertainty in deep learning: International Conference on Machine Learning, **48**, 1050-1059.

Goodfellow, I., Y. Bengio, and A. Courville, 2016, Deep learning: MIT Press.

Graves, A., 2011, Practical variational inference for neural networks: Conference on Advances in Neural Information Processing Systems, 2348–2356.

Guitton, A., 2018, 3D convolutional neural networks for fault interpretation: 80th Annual International Conference and Exhibition, EAGE, Extended Abstracts, 1–5.

Kingma, D. P., and J. Ba, 2015, Adam: A method for stochastic optimization: International Conference on Learning Representations.

Krizhevsky, I. S., G. Hinton, 2012, ImageNet classification with deep convolutional neural networks: Communications of the ACM, **60**, no. 6, 84-90, doi: 10.1145/3065386.

Li, F., H. Zhou, Z. Wang, and X. Wu, 2021, ADDCNN: An Attention-Based Deep Dilated Convolutional Neural Network for Seismic Facies Analysis With Interpretable Spatial–Spectral Maps: IEEE Transactions on Geoscience and Remote Sensing, **59**, no. 2, pp. 1733-1744, doi: doi: 10.1109/TGRS.2020.2999365.

Oktay, O., J. Schlemper, L. L. Folgoc, M. J. Lee, M. Heinrich, K. Misawa, K. Mori, S. G. McDonagh, N. Hammerla, B. Kainz, B. Glocker, and D. Rueckert, 2018, Attention U-net: Learning where to look for the pancreas: Conference on Medical Imaging with Deep Learning.

Schlemper, J., O. Oktay, L. Chen, J. Matthew, C. Knight, B. Kainz, B. Glocker, and D. Rueckert, 2018, Attention-gated networks for improving ultrasound scan plane detection: Conference on Medical Imaging with Deep Learning.

Li, C., Y. Tan, W. Chen, X. Luo, Y. Gao, X. Jia, Z. Wang, 2020, Attention UNet++: A nested attention-aware U-Nnet for liver CT image segmentation: IEEE International Conference on Image Processing, 345-349, doi: 10.1109/ICIP40778.2020.9190761.

Lubo-Robles, D., and K. J. Marfurt, 2019, Independent component analysis for reservoir geomorphology and unsupervised seismic facies classification in the Taranaki Basin, New Zealand: Interpretation, **7**, no. 3, SE19–SE42, doi: 10.1190/INT-2018-0109.1.

Mohri, M., A. Rostamizadeh, and A. Talwalkar, 2012, Foundations of Machine Learning: The MIT Press ISBN 9780262018258.

Napoli, O. O., and V. Martins do Rosario, J. P. Navarro, P. M. C. Silva, and E. Borin, 2020, Accelerating Multi-attribute Unsupervised Seismic Facies Analysis With RAPIDS: ArXiv, abs/2007.15152.

Ovadia, Y., E. Fertig, J. Ren, Z. Nado, D. Sculley, S. Nowozin, J. V. Dillon, B. Lakshminarayanan, J. Snoek, 2019, Can you trust your model's uncertainty? Evaluating predictive uncertainty under dataset shift: Conference on Neural Information Processing Systems.

Ronneberger, O., P. Fischer, and T. Brox, 2015, U-net: Convolutional networks for biomedical image segmentation, in International Conference on Medical image computing and computer-assisted intervention. Springer, pp. 234–241.

Roy, A., A. S. Romero-Peláez, T. J. Kwiatkowski, and K. J. Marfurt, 2014, Generative topographic mapping for seismic facies estimation of a carbonate wash, Veracruz Basin, southern Mexico: Interpretation, **2**, no. 1, SA31–SA47, doi: 10.1190/INT-2013-0077.1.

Saggaf, M. M., M. N. Toksöz, and M. I. Marhoon, 2003, Seismic facies classification and identification by competitive neural networks: Geophysics, **68**, no. 6, 1984–1999, doi: 10.1190/1.1635052.

Salimans, T., I. Goodfellow, W. Zaremba, V. Cheung, A. Radford, and X. Chen, 2016, Improved techniques for training GANs: 30th Annual Conference on Neural Information Processing Systems, 2234–2242.

Saraswat, P., and M. K. Sen, 2012, Artificial immune-based self-organizing maps for seismic facies analysis: Geophysics, **77**, no. 4, O45–O53, doi: 10.1190/geo2011-0203.1.

Shi, Y., X. Wu, and S. Fomel, 2019, SaltSeg: Automatic 3D salt segmentation using a deep convolutional neural network: Interpretation, **7**, no. 3, SE113–SE122, doi: 10.1190/INT-2018-0235.1

Strecker, U., and R. Uden, 2002, Data mining of 3D poststack seismic attribute volumes using Kohonen self-organizing maps: The Leading Edge, **21**, no. 10, 1032–1037, doi: 10.1190/1.1518442.

Singh, S., A. I. Kanli, S. Sevgen, 2016, A general approach for porosity estimation using artificial neural network method: a case study from Kansas gas field: Studia Geophysica et Geodaetica, **60**, no. 1, 130-140.

Singh, S., I. Tsvankin, and E. Zabihi Naeini, 2021, Elastic FWI for orthorhombic media with lithologic constraints applied via machine learning, Geophysics (in print), doi: 10.1190/geo2020-0512.1.

Wen, Y., P. Vicol, J. Ba, D. Train, R. Grosse, 2018, Flipout: Efficient pseudo-independent weight perturbations on mini-batches: 6th International Conference on Learning Representations.

West, B. P., S. R. May, J. E. Eastwood, and C. Rossen, 2002, Interactive seismic facies classification using textural attributes and neural networks: The Leading Edge, **21**, no 10, 1042–1049, doi: 10.1190/1.1518444.

Wrona, T., I. Pan, R. L. Gawthorpe, and H. Fossen, 2018, Seismic facies analysis using machine learning: Geophysics, **83**, no. 5, O83–O95, doi: 10.1190/geo2017-0595.1.

Wu, Y., and K. He., 2018, Group normalization: European Conference on Computer Vision.

Zhao, T., F. Li, and K. J. Marfurt, 2017, Constraining self-organizing map facies analysis with stratigraphy: An approach to increase the credibility in automatic seismic facies classification: Interpretation, **5**, no. 2, T163–T171, doi: 10.1190/INT-2016-0132.1.

Zhao, T., 2018, Seismic facies classification using different deep convolutional neural networks: 88th Annual International Meeting, SEG, Expanded Abstracts, 2046–2050, doi: 10.1190/segam2018-2997085.1.